

A thermoregulation model for whole body cooling hypothermia

Ana Beatriz de C.G. e Silva^{a,1,*}, Luiz C. Wrobel^b, Fernando L.B. Ribeiro^a

^a*Civil Engineering Program, COPPE/Federal University of Rio de Janeiro Technological Center, Ilha do Fundão, CEP 21945-970, Rio de Janeiro, Brazil*

^b*Institute of Materials and Manufacturing, Brunel University London, Uxbridge UB8 3PH, United Kingdom*

Abstract

This paper presents a thermoregulation model based on the finite element method to perform numerical analyses of brain cooling procedures as a contribution to the investigation on the use of therapeutic hypothermia after ischemia in adults. The use of computational methods can aid clinicians to observe body temperature using different cooling methods without the need of invasive techniques, and can thus be a valuable tool to assist clinical trials simulating different cooling options that can be used for treatment. In this work, we developed a finite element method (FEM) package using isoparametric linear three-dimensional elements which is applied to the solution of the continuum bioheat Pennes equation. Blood temperature changes were considered using a blood pool approach and a lumped analysis for intravascular catheter methods of blood cooling. Some analyses are performed using a three-dimensional mesh based on a complex geometry obtained from computed tomography medical images, considering a cooling blanket and an intravascular catheter. A comparison is made between the results obtained with the two techniques and the effects of each case in brain temperature reduction in a required period of time, maintenance of body temperature at moderate hypothermia levels and gradual

*Corresponding author

Email addresses: anabeatrizgonzaga@coc.ufrj.br (Ana Beatriz de C.G. e Silva),
luiz.wrobel@brunel.ac.uk (Luiz C. Wrobel), fernando@coc.ufrj.br (Fernando L.B. Ribeiro)

¹Tel.: +55 (21) 988406995

rewarming.

Keywords: thermoregulation, hypothermia, brain cooling, intravascular catheter, finite element method

1 **1. Introduction**

2 Therapeutic hypothermia is a medical treatment used to reduce the damages
3 caused by ischemic diseases that lead to a hypoxic condition in the internal
4 organs. The brain is the most vulnerable organ to this condition [Tisherman
5 and Sterz, 2005], which can be caused by cardiac arrest, arteries occlusion and
6 cerebral trauma. After an hypoxic-ischemic event, also called primary phase of
7 energy failure, cerebral oxidative metabolism is restored [Christiansen, Rakhilin,
8 Tarakanova, and Wong, 2010]. However, a second energy failure phase may oc-
9 cur in the first few hours after the ischemia, and there is a critical time when
10 secondary factors such as hypotension, hypoxia, hyperglycemia and hyperther-
11 mia may occur and cause brain cell damage [Hickey and J.Painter, 2006]. The
12 window for hypothermic treatment occurs between the primary and secondary
13 energy failure stages, and consists in reducing the brain temperature to a mild
14 ($35 - 36^{\circ}C$) or moderate ($32 - 35^{\circ}C$) hypothermic state, depending on the type
15 of intervention. This reduction results in a decrease of metabolic activities and
16 other hazardous biochemical effects, offering protection and limiting the damage
17 in the affected tissues.

18 In animal trials, an improvement of neurological sequels was observed after
19 hypothermia treatment within six hours of injury [Eicher, Wagner, Katikaneni,
20 Hulse, Bass, Kaufman, Horgan, Languani, Bhatia, Givelichian, Sankaran, and
21 Yager, 2005], even when only a small reduction ($1 - 2^{\circ}C$) is achieved [Diao,
22 Zhu, and Wang, 2003]. Nozari *et al.* [Nozari, Safar, Stezoski, Wu, Kostel-
23 nik, Radovsky, Tisherman, and Kochanek, 2006] state that mild or moderate
24 hypothermia induced during cardiopulmonary resuscitation opens a window of

25 time to restore spontaneous circulation, minimizes organ injury and enables
26 intact survival in dogs.

27 For adults, the most usual type of hypothermia treatment is whole body
28 cooling (WBC) using thermal blankets and thermal mattresses, the application
29 of ice pads, intracarotid infusion of cold fluid or intravascular catheter. The
30 efficacy of each method is still under discussion, as there is no consensus so far
31 about which of them would have a better effect in reducing sequels.

32 Multiple studies also suggest that, after the treatment, a gradual rewarming
33 phase is really important. Zhu *et al.* [Zhu, Schappeler, Cordero-Tumangday,
34 and Rosengart, 2009] state that rapid rewarming may result in rebound intracra-
35 nial pressure elevation to dangerous levels and reduction of cerebral perfusion
36 pressure, worsening outcome in brain injuries, emphasizing the importance of
37 a gradual rewarming. For this reason, it is suggested that the process should
38 be conducted at a rate of less than $0.5^{\circ}C/h$ [Hoque, Chakkarapani, Liu, and
39 Thoresen, 2010].

40 In recent years, different models were developed to simulate the human ther-
41 moregulatory behaviour, from two-node models of core and skin heat balances to
42 more complex multi-segment models of the human body and its thermoregula-
43 tory responses [Fiala, Lomas, and Stohrer, 1999]. The latter model incorporates
44 concepts of physiological regulation to predict human thermal responses and
45 body heat loss at various activity levels and thermal environments [Al-Othmani,
46 Ghaddar, and Ghali, 2008]. Practical examples can be found in different appli-
47 cations [Kingma, Vosselman, Frijns, Steenhoven, and Lichtenbelt, 2014, Fiala,
48 Lomas, and Stohrer, 1999, Al-Othmani, Ghaddar, and Ghali, 2008].

49 Early attempts to develop head cooling models did not consider arterial tem-
50 perature changes [Dennis et al., 2003, Leeuwen et al., 2000]. According to Zhu
51 and Diao [2001], the arterial temperature is the major determinant of the tem-
52 perature in the body tissues, being responsible for a protective effect against
53 external cooling. The blood flow in the circulatory system is responsible for the
54 thermoregulation in the tissues. During hypothermia, hyperthermia or changes
55 in the environment, it works regulating the local temperature [Bhowmik, Singh,

56 Repaka, and Mishra, 2013]. As the arterial temperature regulates the local
57 tissue temperature, hypothermia simulation models must consider arterial tem-
58 perature changes. The work of Al-Othmani *et al.* [Al-Othmani, Ghaddar, and
59 Ghali, 2008] uses an arterial system model to calculate blood flow in the core
60 tissue and a bioheat model to determine skin temperature for nude and clothed
61 human bodies in transient non-uniform environments. The model presented in
62 [Fiala, 1998] incorporates the body heat losses considering a non-uniform tem-
63 perature distribution in the skin, regulatory responses, properties of clothing
64 used and various environmental conditions such as extreme temperatures, wind
65 speed and solar radiation. Xiang and Liu [Xiang and Liu, 2008] use a com-
66 partmental model of 12 body segments and a blood compartment to simulate
67 whole body hyperthermia treatments for tumours. In [Laszczyk and Nowak,
68 2015b, Silva, Laszczyk, Wrobel, Ribeiro, and Nowak, 2016], a heat transfer
69 model was implemented to simulate hypothermia treatment in neonates using a
70 three-dimensional geometry obtained from magnetic resonance imaging (MRI)
71 scans. In [Zhu, Schappeler, Cordero-Tumangday, and Rosengart, 2009], a nu-
72 merical model for whole body intravascular cooling was developed and applied to
73 a human body consisting of a cylinder of one material and a combination of com-
74 ponents representing torso, head and limbs. The work calculated a $1.2^{\circ}C/hour$
75 cooling rate for a cooling capacity of $100W$ and suggested the method can be
76 used to reduce critical fever of $40^{\circ}C$ or hypothermia of $34^{\circ}C$ in less than 3
77 hours.

78 For the rewarming phase of the hypothermia therapy, the simulation of the
79 rewarming procedure by [Diao, Zhu, and Wang, 2003] considering a passive
80 rewarming, taking off the helmet or icepacks and considering the room temper-
81 ature of $25^{\circ}C$, showed the need for more studies in this part of the procedure, as
82 the passive rewarming in this case was too rapid. Some studies using a mattress
83 to simulate hyperthermia conditions [Vallez, Plourde, and Abraham, 2016] used
84 experimental data to determine some parameters that can be used not only on
85 the rewarming stage but also during the whole procedure of hypothermia using
86 a cooling mattress.

87 In this work, the Pennes bioheat equation was used to simulate bioheat
88 transfer in the human body, and the model that represents heat exchange on
89 the circulatory system described in [Fiala, 1998] was implemented in a three-
90 dimensional finite element code to simulate hypothermia treatments in adults.
91 The in-house software was developed at the Structure and Materials Labora-
92 tory at the Federal University of Rio de Janeiro, as a continuation of the work
93 of [Silva, 2012, 2016]. Numerical analyses of whole body cooling methods were
94 performed to compare the efficacy of cooling mattress and intravascular catheter
95 procedures during rapid cooling, maintenance of cooling and rewarming phase
96 of the therapy. A thermoregulation model capable of simulating a real cooling
97 therapy can be used to assist clinical trials for hypothermia techniques, sim-
98 ulating the best options to be used during treatment and improving low cost
99 methods that could be used in hospitals and clinics that cannot afford expensive
100 techniques.

101 2. Methodology

102 2.1. Bioheat Transfer

103 In this paper, the calculation of a whole body thermal analysis will be based on
104 a blood perfusion continuum macro-scale bioheat model developed by Pennes
105 [Bhowmik, Singh, Repaka, and Mishra, 2013]:

$$\rho_t c_t \frac{\partial T_t}{\partial t} = \nabla \cdot (k_t \nabla T_t) + \rho_b c_b \omega_b (T_a - T_t) + \dot{q}_m \quad (1)$$

106 and represents the bioheat flux in a domain Ω . The symbol T is the temperature
107 and the subscripts t , b , a and m represent tissue, blood, arterial blood and
108 metabolism, respectively. The material properties defined in the equation are:
109 k (thermal conductivity), c (specific heat), ρ (density) and ω (blood perfusion
110 rate). The metabolic heat generation rate is represented by \dot{q}_m . The values of
111 the parameters will be defined in the next section.

112 For each tissue of the body are defined different properties. Prescribed tem-
113 peratures $\bar{T}(\Gamma_t, t)$ in the boundary Γ_t and heat fluxes $\bar{q}(\Gamma_q, t)$ in the boundary

114 Γ_q are defined as boundary conditions in the boundary $\Gamma = \Gamma_t \cup \Gamma_q$. The initial
 115 condition is

$$T(x, t_0) = T_0, \quad (2)$$

116 where T_0 is the initial temperature in each tissue, which may vary according to
 117 the position within the body.

118

119 2.2. Metabolism

120

121 The metabolic heat generation rate in each tissue is composed of the basal
 122 rate $\dot{q}_{m,0}$, and an additional rate $\Delta\dot{q}_m$ generated by a local thermoregulation
 123 activity [Fiala, 1998]:

$$\dot{q}_m = \dot{q}_{m,0} + \Delta\dot{q}_m \quad (3)$$

124 The rate $\Delta\dot{q}_m$ is composed of three terms:

$$\Delta\dot{q}_m = \Delta\dot{q}_{m,0} + \Delta\dot{q}_{m,sh} + \Delta\dot{q}_{m,w} \quad (4)$$

125 where the local basal metabolic variation is $\Delta\dot{q}_{m,0}$ and variations due to changes
 126 in metabolism are represented by the terms $\Delta\dot{q}_{m,sh}$ and $\Delta\dot{q}_{m,w}$. These variations
 127 are caused by shivering and muscular effort, and occurs only in muscular tissues.
 128 The local basal metabolic variation can be calculated by [Fiala, Lomas, and
 129 Stohrer, 1999]:

$$\Delta\dot{q}_{m,0} = \dot{q}_{m,0} [Q_{10}^{\frac{T_t - T_0}{10}} - 1] \quad (5)$$

130 where T_0 is the temperature of thermal neutrality, equal to $30^\circ C$ and the Q_{10}
 131 coefficient is responsible for changes in the metabolic heat generation rate and
 132 blood perfusion rate due to changes in the temperature of the tissues, defined
 133 from experimental measurements to be in a range between 2 and 4 and usually
 134 considered as equal to 2 [Fiala, Havenith, Bröde, and B. Kampmann, 2012].
 135 The shivering effect may be neglected because it may be controlled in a medical

136 procedure for adults. The muscular response may also be omitted since the
137 hypothermia treatment does not involve muscular activities that may increase
138 the metabolic heat generation at a significant level.

139 *2.3. Arterial Temperature*

140

141 In Eq. (1) the term that represents the blood perfusion considers that the
142 heat exchange between blood and tissues occurs only on the capillary vessels,
143 but adjacent arteries and veins exchange heat in the body extremities, where
144 the blood is colder than in the core. These effects must be considered in the
145 model, as the tissue temperature influences the arterial blood temperature. To
146 take this effect into account the arterial temperature calculation is performed by
147 a circulatory system model described in [Fiala, 1998, Silva, Laszczyk, Wrobel,
148 Ribeiro, and Nowak, 2016].

149 This model assumes that the arterial temperature has different values in
150 different regions of the human body, called sectors. The central sectors have
151 an arterial temperature equal to the blood pool temperature while the arterial
152 temperature of the extremities is influenced by the countercurrent heat exchange
153 effect. Assuming mass continuity in blood vessels and the net flow rate from the
154 equation of Gordon [Gordon, 2001], the arterial temperature can be calculated
155 as:

$$T_a = \frac{\dot{m}_b c_b T_p + h_x T_v}{\dot{m}_b c_b + h_x} \quad (6)$$

156 In the above equation, T_p is the blood pool temperature, T_a and T_v are the
157 arterial and venous temperatures and h_x is the counter current heat exchange
158 coefficient, considered as zero in the core and with defined values obtained from
159 experimental measurements for the extremities of the body [Fiala, Lomas, and
160 Stohrer, 1999].

161 As the bioheat equation assumes capillary blood is in equilibrium with the
162 surrounding tissue[Fiala, 1998], the calculation of T_v in a body element can be

163 obtained as follows:

$$T_{v_{element}} = \frac{\int \omega_b T_t dV}{\int \omega_b dV} \quad (7)$$

164 This means the venous blood leaving the body element is equal to the local
165 tissue temperature of the element.

166 The implementation presented here is similar to the model applied for neonates
167 described in [Laszczyk and Nowak, 2015a, Silva, Laszczyk, Wrobel, Ribeiro, and
168 Nowak, 2016], and is a fully continuum three-dimensional model that considers
169 that all sectors of the body are connected and all surfaces exchange heat. The
170 numerical procedure to calculate T_a , T_v and T_p will be shown in Section 2.7.

171 2.4. Blood Perfusion Rate

172 The blood perfusion rate $\omega_{b,t}$ in a specific tissue can be described as a com-
173 position of two terms:

$$\omega_{b,t} = \omega_{b,0,t} + \Delta\omega_{b,t} \quad (8)$$

174 where $\omega_{b,0,t}$ stands for the local basal blood perfusion rate and $\Delta\omega_{b,t}$ is a local
175 temperature-dependent variation. Assuming that the local blood perfusion rate
176 is coupled with the local metabolic heat generation [Diao, Zhu, and Wang, 2003],
177 this local variation may be calculated as:

$$\Delta\omega_{b,t} = \omega_{b,0,t} \left[Q_{10}^{\frac{T_t - T_0}{10}} - 1 \right] \quad (9)$$

178 Similarly to Eq.(5), the reference temperature T_0 is the temperature of thermal
179 neutrality and the Q_{10} coefficient is usually considered as equal to 2.

180

181 2.5. External Heat Exchange

182 The external heat exchange is sum of the contributions of three main mech-
183 anisms: convection, radiation and evaporation. The heat exchange rate varies

184 along the body surface, and the heat flux consists of the convective, radiative
 185 and evaporative fluxes:

$$q_{skin} = q_{conv} + q_{rad} + q_{evap} \quad (10)$$

186 The convective flux q_{conv} between the environment and the body boundaries
 187 consists of the skin surface and it can be obtained using the Newton cooling law,
 188 defined as

$$q_{conv} = h_{conv} \cdot (T_{ext} - T_{skin}) \quad (11)$$

189 The symbol T_{ext} represents the external air temperature and h_{conv} is the con-
 190 vective heat transfer coefficient.

191 The radiative flux is calculated using the Stefan-Boltzmann law:

$$q_{rad} = h_{rad}(T_{skin}^4 - T_{sr,mean}^4) \quad (12)$$

192 where T_{skin} , $T_{sr,mean}$ and h_{rad} are the temperatures at the skin surface, the
 193 temperature of the radiation source on the exterior of the domain, and a radia-
 194 tive parameter, respectively, and

$$h_{rad} = \sigma \varepsilon \quad (13)$$

195 in which σ refers to the Stefan-Boltzmann constant and ε is the emissivity of
 196 the external skin surface. The value of the emissivity varies according to the
 197 surface material.

198 The evaporative flux was incorporated in the model as a prescribed heat
 199 flux boundary condition to consider heat losses by evaporation, based on values
 200 described in the literature. In the applications described in this paper the
 201 basal evaporation rate from the skin was considered as $18W$ (taken from [Fiala,
 202 Havenith, Bröde, and B. Kampmann, 2012]).

203 Respiration losses were incorporated on the material thermal properties of
 204 the trunk/head sectors, as respiration can be responsible for a loss of 25% of
 205 whole-body metabolic heating [Vallez, Plourde, and Abraham, 2016].

206 The value of the external heat transfer coefficient may be adjusted to simu-
207 late clothed or unclothed situations as discussed in [Al-Othmani, Ghaddar, and
208 Ghali, 2008].

209

210 *2.6. Lumped Analysis for Blood Cooling*

211 One of the most effective ways to reduce body temperature is to use in-
212 travascular cooling catheters that directly cool the major veins and can achieve
213 cooling rates of $5.0^{\circ}C/hour$ depending on the capacity of the device [Dae, Gao,
214 Ursell, Stillson, and Sessler, 2003]. In these procedures, the blood temperature is
215 actively lowered or increased. The simulation of blood cooling for hypothermia
216 treatments using methods applied directly to the blood vessels, as intravenous
217 saline fluid infusion or an intravascular catheter, needs an additional equation
218 coupled to the Pennes bioheat equation to account for the tissue-blood thermal
219 interactions.

220 The model implemented in this paper considers the energy balance of a
221 blood compartment as a lumped system that combines the energy added or
222 subtracted by an external device and the loss of heat from blood to tissues during
223 circulation. This model, adapted from [Zhu, Schappeler, Cordero-Tumangday,
224 and Rosengart, 2009], provides a method to obtain blood and body temperatures
225 during active blood temperature modifications and is capable of simulating the
226 stages of cooling and rewarming of blood during hypothermia procedures to
227 treat strokes and brain damages in adults.

228 The mathematical model consists of a coupled simulation of body temper-
229 ature distribution and blood energy balance, and couples the Pennes bioheat
230 equation (Eq. 1) and an equation of energy balance of the blood compartment
231 of the body to predict blood temperature change during clinical applications.
232 Because of the relatively short recalculation time, blood in the human body is
233 represented as a lumped system. The governing equation for the blood temper-
234 ature can be written as [Zhu, Schappeler, Cordero-Tumangday, and Rosengart,

235 2009]

$$\rho_b c_b V_b \frac{dT_a}{dt} = Q_{ext}(T_a, t) - Q_{b-t}(t) = Q_{ext}(T_a, t) - \rho_b c_b \bar{\omega} V_{body} (T_a - \bar{T}_t) \quad (14)$$

236 where Q_{ext} represents the capacity of the external device and can be a function
 237 of arterial temperature or time, and V_{body} stands for the volume of the body.
 238 The parameter $\bar{\omega}$ is the mean volumetric blood perfusion rate, calculated by:

$$\bar{\omega} = \frac{1}{V_{body}} \iiint_{V_{body}} \omega dV_{body} \quad (15)$$

239 and \bar{T}_t is the weight-average tissue temperature, defined by the relation:

$$\rho c \omega (T_{a0} - \bar{T}_t) V_{body} = \iiint_{V_{body}} \rho c \omega (T_{a0} - T_{t0}) dV_{body} \quad (16)$$

240 where T_{a0} stands for the arterial temperature before time step $t + \Delta t$ and T_{t0}
 241 represents the tissue temperature before time step $t + \Delta t$. At steady-state,
 242 the arterial temperature T_a should be the same as the weight-average tissue
 243 temperature \bar{T}_t .

244 The numerical procedure for the implementation of this model will be shown
 245 in the next section.

246 2.7. Numerical Model

247 The solution of the Pennes bioheat equation and the circulatory model de-
 248 scribed in section 2.4 is obtained using the finite element method The transient
 249 problem is solved using a time-marching scheme based on a semi-discrete form
 250 of the finite element method (FEM). The numerical model is described in [Silva,
 251 Laszczyk, Wrobel, Ribeiro, and Nowak, 2016]. Considering Eq. (1) in a spa-
 252 tial domain Ω and a temporal interval $(0, \Pi)$, the domain Ω is discretized into
 253 elements and at each time step $t = t_{n+1}$, the following system of algebraic
 254 equations is obtained:

$$M \dot{T}_{n+1} + K T_{n+1} = F_{n+1} \quad (17)$$

255 where M is the mass matrix, \dot{T}_{n+1} stands for the nodal values of the time deriva-
 256 tive of temperature, K is the stiffness matrix, T_{n+1} are the nodal temperatures
 257 at time step t_{n+1} and F_{n+1} is the vector of independent terms. The coefficients
 258 of these matrices are calculated as follows:

$$m_{ij} = \int_{\Omega} c_t \rho_t N_i N_j d\Omega \quad (18)$$

259

$$K_{ij} = k_t \int_{\Omega} \left(\frac{\partial N_i}{\partial x} \frac{\partial N_j}{\partial x} + \frac{\partial N_i}{\partial y} \frac{\partial N_j}{\partial y} + \frac{\partial N_i}{\partial z} \frac{\partial N_j}{\partial z} \right) d\Omega + \int_{\Omega} c_b \rho_b \omega_b N_i N_j d\Omega \quad (19)$$

260

$$f_i = \int_{\Omega} \dot{q}_m N_i d\Omega - \int_{\Gamma} \bar{q} N_i d\Gamma + \int_{\Omega} c_b \rho_b \omega_b T_a N_i d\Omega \quad (20)$$

261 The counter current heat exchange effect and the changes in arterial tem-
 262 perature are calculated for each sector $T_{a,l}$ as

$$T_{a,l} = \frac{\rho_b c_b \left(\sum_{i=1}^{N_l} \omega_{b,t,l} V_{i,t,l} \right) T_p + h_{x,l} T_{v,l}}{\rho_b c_b \left(\sum_{i=1}^{N_l} \omega_{b,t,l} V_{i,t,l} \right) + h_{x,l}} \quad (21)$$

263 where the subscript l denotes the sector of the body, the number of elements in
 264 each sector l is denoted by N_l and the volume of element i of the tissue t in the
 265 sector l is $V_{i,t,l}$.

266 As the venous temperature of each element is equal to the tissue tempera-
 267 ture, to calculate the venous temperature $T_{v,l}$ in each sector, Eq. (7) can be
 268 incorporated to the numerical model as:

$$T_{v,l} = \frac{\rho_b c_b \left(\sum_{i=1}^{N_l} \omega_{b,t,k} V_{i,t,l} T_{i,t,l} \right)}{\rho_b c_b \left(\sum_{i=1}^{N_l} \omega_{b,t,l} V_{i,t,l} \right)} \quad (22)$$

269 The blood pool temperature can be written as:

$$T_p = \frac{\sum_{l=1}^L \left[\frac{\rho_b c_b \left(\sum_{i=1}^{N_l} \omega_{b,t,l} V_{i,t,l} \right) \rho_b c_b \left(\sum_{i=1}^{N_l} \omega_{b,t,l} V_{i,t,l} T_{i,t,l} \right)}{\rho_b c_b \left(\sum_{i=1}^{N_l} \omega_{b,t,l} V_{i,t,l} \right) + h_{x,l}} \right]}{\sum_{l=1}^L \left[\frac{\left[\rho_b c_b \left(\sum_{i=1}^{N_l} \omega_{b,t,l} V_{i,t,l} \right) \right]^2}{\rho_b c_b \left(\sum_{i=1}^{N_l} \omega_{b,t,l} V_{i,t,l} \right) + h_{x,l}} \right]} \quad (23)$$

270 where L is the total number of sectors in the body and $T_{i,t,l}$ is the temperature
 271 of each element i of tissue t in sector l . For the treatment of the non-linearities
 272 a predictor multi-corrector algorithm was used [Hughes, 1987], as described in
 273 [Silva, Laszczyk, Wrobel, Ribeiro, and Nowak, 2016].

274 For the method described in section 2.7 for blood cooling applications in
 275 adults, the transient problem represented by Eq. (14) can be discretized by
 276 finite differences. The implicit discretization scheme results in the calculation
 277 of the arterial temperature as:

$$T_a^{n+1} = \frac{\frac{Q_{ext} \Delta t}{\rho_b c_b V_b} + T_a^n + \overline{T_t^n} \left(\frac{\rho_b c_b \bar{\omega} V_{body} \Delta t}{\rho_b c_b V_b} \right)}{1 + \frac{\rho_b c_b \bar{\omega} V_{body} \Delta t}{\rho_b c_b V_b}} \quad (24)$$

278 In this case, the same iterative solver and element calculation procedures of the
 279 previous model is used. The calculation of the temperature T_a^{n+1} is performed
 280 before step 5 at each new time step.

281 3. Applications

282 The geometrical model used for simulations of adults was obtained by seg-
 283 mentation of 3D medical images (CT scans) of the Visible Human Data Set
 284 (VHD) provided by the National Library of Medicine, US Department of Health
 285 and Human Services. The medical images were used to generate the geometry
 286 using the software *MIMICS* and adapted using the packages *ANSYS Workbench*

287 and *Trelis* to generate a 13 million mesh of a male adult with a body weight of
288 $100kg$, body surface area of $2.27m^2$, $1.88m$ height, a cardiac output of $6l/min$
289 and 28% body fat content. The total basal whole body metabolism is $106W$
290 and basal evaporation rate from the skin of $18W$ (taken from [Fiala, Havenith,
291 Bröde, and B. Kampmann, 2012]). The simulations were performed using a
292 platform comprised by two Xeon *E5 – 5420* processors with $64GB$ of RAM and
293 12 cores.

294 The geometry of the body is composed of eight different materials: skin+fat,
295 muscle, bone, brain, viscera, lungs, eyes and cerebrospinal fluid). For the cal-
296 culation of the arterial temperature, the body is divided in six sectors: trunk
297 + abdomen, head, arm, hand, leg, foot. The simulations where performed in a
298 geometry of half of the body, due to symmetry. The materials and division into
299 sectors are depicted in Figures 1-4.

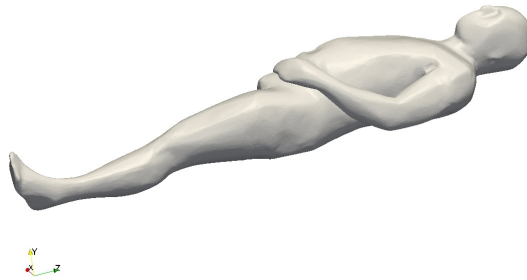


Figure 1: Geometry of the male adult

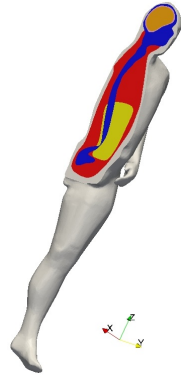


Figure 2: Geometry of the male adult, internal organs

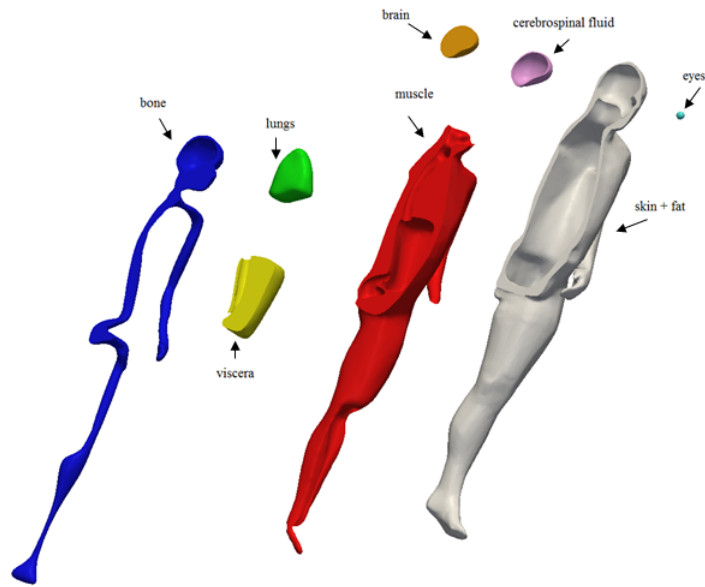


Figure 3: Geometry of the tissues

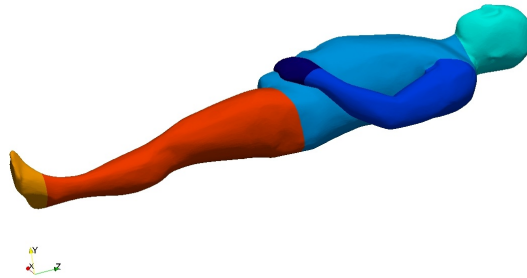


Figure 4: Division into sectors

300 The finite element mesh consisted of 13 million four-node tetrahedral ele-
 301 ments. A zoom in the upper region of the body is shown in Figure 5.

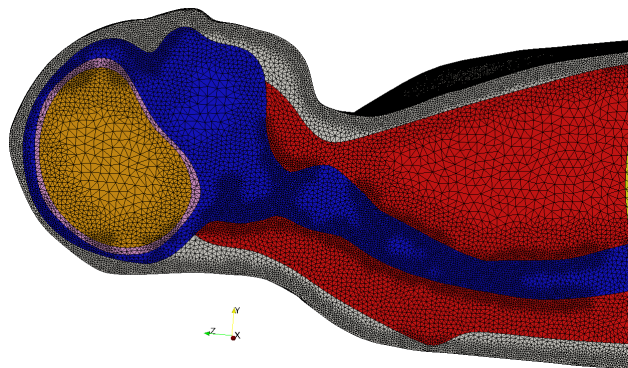


Figure 5: Zoom -Mesh of 13.0 million elements

302 The thermophysiological properties of the human tissues were taken from
 303 the literature, adapted from [Vallez, Plourde, and Abraham, 2016, Fiala, 1998,
 304 Hasgall, Gennaro, Baumgartner, Neufeld, Gosselin, Payne, Klingenbock, and
 305 Kuster, 2015]. Table 1 shows the tissue thermophysiological properties used in
 306 this simulation. Metabolic heat generation rates used in the simulation consider
 307 the impact of respiration on heat loss corresponding to 25% of the whole-body
 308 metabolic heating [Vallez, Plourde, and Abraham, 2016], distributed over the
 309 elements belonging to the sectors trunk+abdomen and head. The counter cur-
 310 rent heat exchange coefficients were taken from [Fiala, 1998] and are presented
 311 in Table 2.

Table 1: Thermophysiological properties of the different tissues

Material properties					
Tissue	Thermal Con- ductivity ($W/m \cdot ^\circ C$)	Density (kg/m^3)	Specific Heat ($J/kg \cdot ^\circ C$)	Metabolic Heat Genera- tion Rate (W/m^3)	Blood Perfusion Rate (1/s)
Blood	0.5	1050	3800	-	-
Eye	0.43	1076	4200	0	0
Lungs	0.39	394	3886	1835	0.0008677
Skin + Fat	0.2	877	2727	170	0.0003146
Cerebrospinal fluid	0.57	1007	380	0	0
Bones	1.16	1300	1590	0	0
Muscle	0.5	1050	3770	528	0.0005355
Viscera	0.55	1100	3350	3160	0.004532
Brain	0.53	1360	2450	12954	0.013124

Table 2: Counter current heat exchange coefficient of the seven sectors of the body

Countercurrent heat exchange coefficient - h_{xc} ($W/^\circ C$)						
Sector	Head	Trunk+Abdomen	Arm	Hand	Leg	Foot
	0.000	0.000	4.13	0.57	6.2	1.45

312 The first example used to validate the adult geometry and tissue properties
313 in these simulations was taken from [Vallez, Plourde, and Abraham, 2016, Fiala,
314 Lomas, and Stohrer, 1999] and consists of a male human in an environment in
315 thermal neutrality. The boundary conditions consist of a convective heat flux at

316 the skin surface (Eq.11). The skin surface was exposed to a room temperature
 317 of $30^{\circ}C$ and a heat transfer coefficient value of $7W/m^2.^{\circ}C$ was used, as defined
 318 in [Vallez, Plourde, and Abraham, 2016, Fiala, Lomas, and Stohrer, 1999].

319 The simulation of the WBC procedure was based on temperature results
 320 found in different clinical studies [Wang, Olivero, Lanzino, Elkins, Rose, and
 321 Honings, 2004, Yang, Ou, and Chen, 2006, Harris, Muh, Surles, Pan, Rozycki,
 322 and Macleod, 2009, Callaway, Tadler, Katz, Lipinski, and Brader, 2002] and the
 323 boundary conditions of the numerical simulations [Fiala, 1998, Vallez, Plourde,
 324 and Abraham, 2016, Laszczyk and Nowak, 2015a] were considered to perform
 325 analyses that match the same values obtained in the clinical trials. The target
 326 was to reduce core temperature to around $34^{\circ}C$ after 1 – 4 hours, maintaining
 327 the temperature at this level during 24 hours and then rewarming the body at
 328 a rate of $0.15 - 1.45^{\circ}C/hour$. Although the body temperature can be higher
 329 or lower than the normal temperature depending on the trauma, the examples
 330 presented in this work consider an initial body temperature of $37^{\circ}C$.

331 Whole body cooling simulations were performed considering a cooling mat-
 332 tress on the bottom part of the body, where convective heat fluxes were pre-
 333 scribed using Eq. 11, and heat transfer to the room environment on the top part,
 334 with convective heat fluxes prescribed using Eq. 11. Evaporative heat fluxes
 335 were also considered on the top part of the body as a prescribed heat flux, cal-
 336 culated using the basal evaporation rate from the skin. For the top part, the
 337 total heat flux at the skin surface is composed by the sum of convective and
 338 evaporative heat fluxes:

$$q_{skin} = q_{conv} + q_{evap} \quad (25)$$

339 and the evaporative heat flux q_{evap} can be calculated according to

$$q_{evap} = \frac{Q_{evap}}{A_{top}} \quad (26)$$

340 where Q_{evap} represents the basal evaporation rate and A_{top} the area of the top
 341 surface of the body. The flux per unit of area was given at each external bound-

342 ary surface element to calculate the equivalent nodal loads. Both boundary
343 regions are depicted in Fig. 6.



Figure 6: Top (green) and bottom (black) surfaces used to prescribe boundary conditions in whole body cooling

344 For the top surface, a room temperature of $25^{\circ}C$ was prescribed and a con-
345 vective heat transfer coefficient of $7W/m^2.^{\circ}C$ is used. The contact between body
346 and cooling mattress is simulated by a convective flux prescribed at the bottom
347 surface, considering an initial temperature of $10^{\circ}C$ during the first 2 hours of
348 analysis. After this initial rapid cooling, the cooling mattress temperature is
349 set to $33^{\circ}C$ during 22 hours. The convective heat transfer coefficient was set
350 to $10W/m^2.^{\circ}C$, based on experimental studies found in [Vallez, Plourde, and
351 Abraham, 2016]. A second subcase was performed considering a room tempera-
352 ture of $20^{\circ}C$ and comparing the results. After 2 hours of simulation the cooling
353 mattress temperature has been set to $34^{\circ}C$ during the rest of the analysis.

354 The third example demonstrates the validity of our model for transient condi-
355 tions. It consists of the simulation of the rewarming phase using the same
356 boundary conditions of the cooling mattress case during 24 hours and then
357 raising the temperature of the mattress. The mattress temperature was set to
358 different values to compare core temperature behaviour. In this case, mattress
359 temperatures of $37^{\circ}C$, $42^{\circ}C$ and $45^{\circ}C$ were used.

360 Test four demonstrates the viability of cooling using an intravascular catheter,
361 with a novel numerical method adapted from [Zhu, Schappeler, Cordero-Tumangday,
362 and Rosengart, 2009], which is used for the first time in a comprehensive whole
363 body cooling model. For this case, the same boundary regions (top and bot-
364 tom) of the previous case are used. The mattress in this case does not exchange
365 heat and is considered as an insulated surface during the first hour of simula-

tion(prescribed heat fluxes at the bottom part are null). After the first hour,
the mattress temperature is set to $33^{\circ}C$ and the heat transfer coefficient of
 $10W/m^2.^{\circ}C$ is used (Eq.11). The top surface is subject to a convective flux
with a heat transfer coefficient of $7W/m^2.^{\circ}C$ (Eq. 11) and a prescribed evap-
orative heat flux based on the basal evaporation rate from the skin.. The heat
exchanged by the device is $100W$ during the first hour of simulation; after this
period, the device is turned off. The idea is to use the device for rapid cool-
ing and then maintain the temperature at a hypothermia level using a cooling
mattress.

4. Results

In the first case, conditions of thermal neutrality were imposed and a tran-
sient simulation was performed until a steady-state solution was obtained. The
core temperature was defined as equal to the blood pool temperature calculated
during the simulation. The core temperature was extracted and compared to
normothermic values of a human subject to a $30^{\circ}C$ room temperature. The
results showed a core temperature of $37^{\circ}C$, in agreement with values from other
studies [Vallez, Plourde, and Abraham, 2016, Fiala, 1998]. The mean skin sur-
face temperature was $34.3^{\circ}C$, consistent with the results of published data for
neutrality conditions described by [Fiala, 1998], where the mean skin surface
temperature of $34.4^{\circ}C$ has been obtained.

The second case analyses core temperature during a whole body cooling
treatment using a cooling mattress. Figure 7 shows changes in blood pool
temperature during the 24 hour procedure.

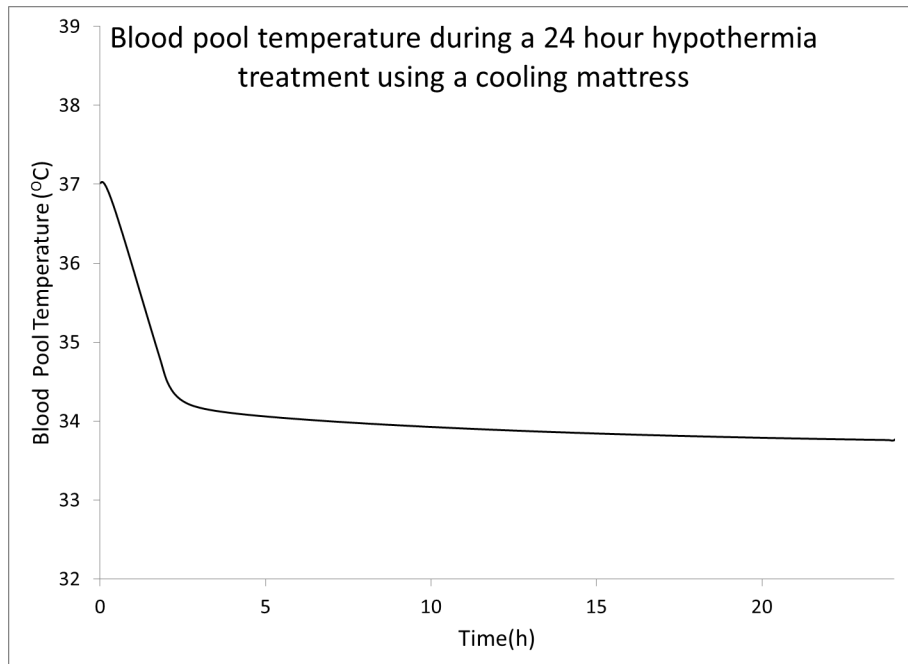


Figure 7: Second case: Core temperature during a 24 hour treatment using a cooling mattress.

389 The results show a drop in the blood pool temperature to 34°C after 2 hours
 390 of simulation and the core temperature reaches the minimum value of 33.8°C
 391 at the end of the simulation. The temperature profile at the end of the analysis
 392 at the outer skin and internal organs is depicted in Fig. 8 and Fig. 9. It should
 393 be noted that the interface between the upper and bottom boundary conditions
 394 is a continuous field, not a step function as may be misinterpreted from Fig. 8

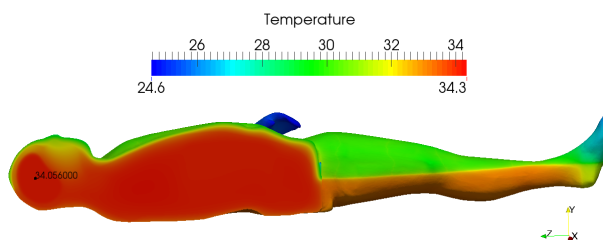


Figure 8: Second case: Internal temperature distribution after a 24 hour treatment.

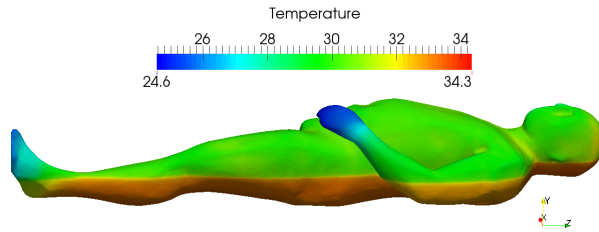


Figure 9: Second case: Skin temperature distribution after a 24 hour treatment.

395 The temperature profile shows a minimum brain temperature of $34.1^{\circ}C$ at
 396 the end of the simulation. The temperature distribution at the top skin surface
 397 has a range between $24.6 - 30^{\circ}C$, and the minimum values are found in the
 398 extremities (hands and feet).

399 The third case analyzes core temperature during the rewarming phase of
 400 the WBC treatment. Three analyses were performed, considering the mattress
 401 temperature set to $37^{\circ}C$, $42^{\circ}C$ and $45^{\circ}C$. Figure 10 shows a comparison be-
 402 tween the blood pool temperature during 7 hours of rewarming for the three
 403 cases analyzed.

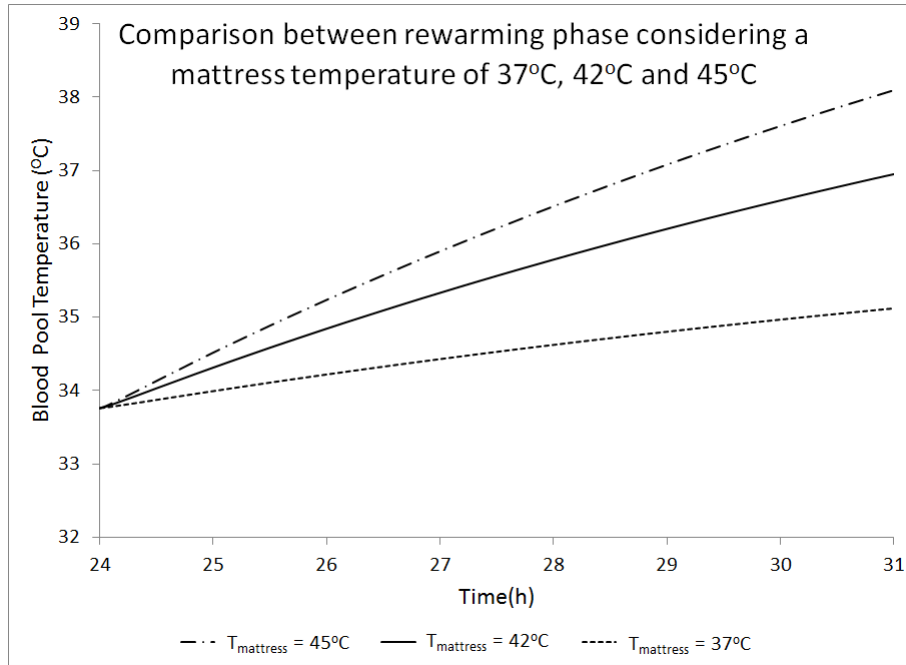


Figure 10: Third case: Comparison between core temperature after a 24 hour hypothermia treatment using different mattress temperatures.

404 The results show a considerable influence of the mattress temperature in
 405 the core temperature during the rewarming phase. The fastest rewarming rate
 406 is $0.63^{\circ}\text{C}/\text{hour}$, for the mattress temperature of 45°C . Rewarming rates of
 407 $0.47^{\circ}\text{C}/\text{hour}$ and $0.20^{\circ}\text{C}/\text{hour}$ were obtained for mattress temperatures of 42°C
 408 and 37°C , respectively. Based on these results, the more suitable rewarming
 409 mattress temperature for a real case is 42°C . The core temperature during the
 410 whole simulation (rapid cooling, cooling and rewarming) for the 42°C rewarming
 411 mattress temperature is shown in Fig. 11.

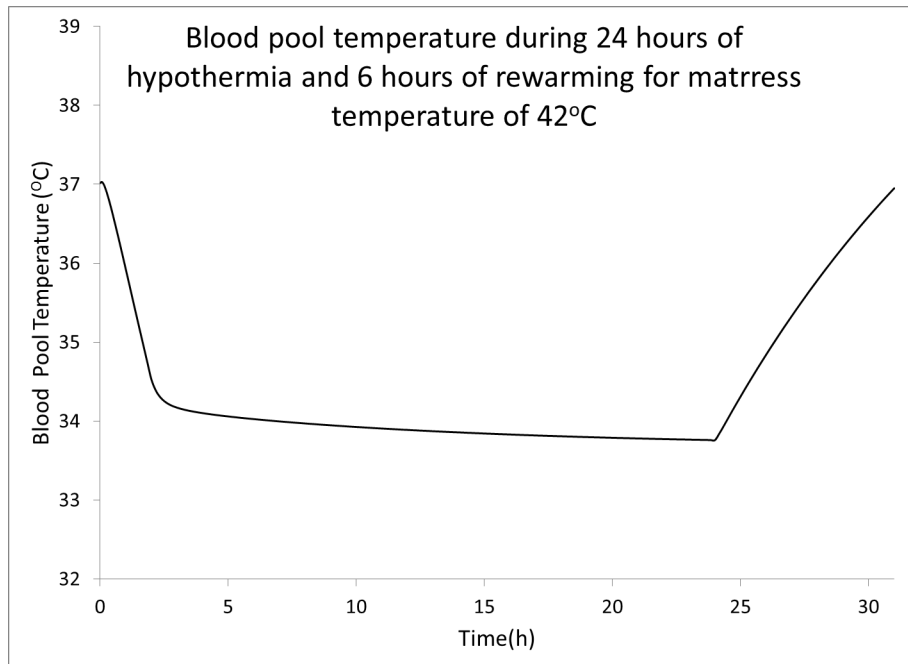


Figure 11: Third case: Core temperature during 24 hours of hypothermia and 6 hours of rewarming for mattress temperature of 42.0°C.

412 The temperature profile at the end of the analysis at the outer skin and
 413 internal organs is depicted in Fig 12 and Fig. 13.

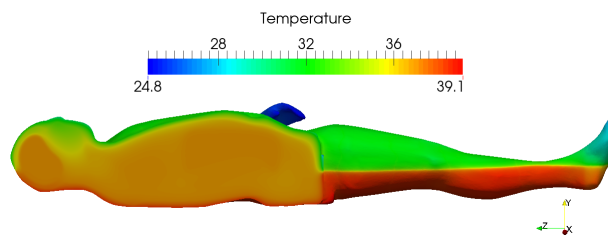


Figure 12: Third case: Internal temperature distribution after rewarming.

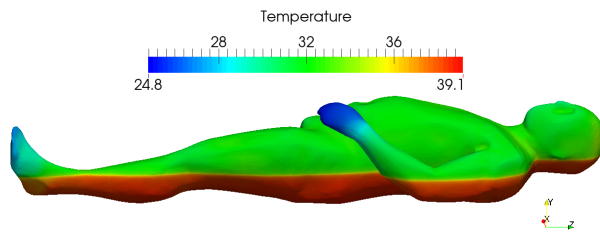


Figure 13: Third case: Skin temperature distribution after rewarming.

414 The temperature profile shows the brain temperature reestablishes the nor-
 415 mothermic value at the end of the simulation. The temperature distribution at
 416 the top skin surface has a range between $24.8 - 32^{\circ}C$, and the minimum values
 417 are found in the extremities (hands and feet).

418 A second simulation using the same parameters and a room external tem-
 419 perature of $20^{\circ}C$ is performed to compare the behaviour and distribution of
 420 temperatures for a decrease in the room temperature of $5^{\circ}C$. The compari-
 421 son between core temperature during rapid cooling, cooling maintenance and
 422 rewarming is plotted in Fig. 14.

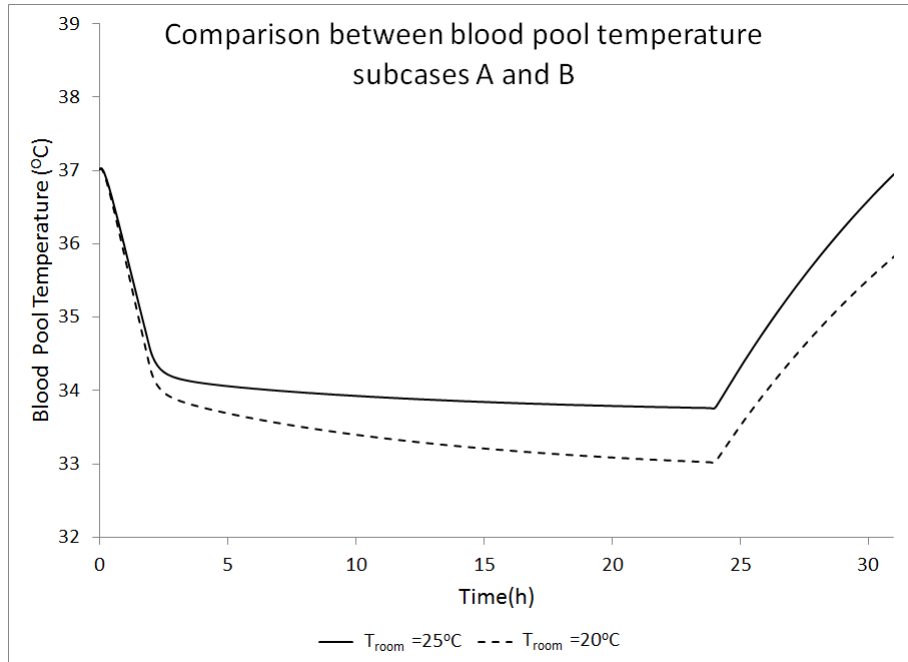


Figure 14: Third case: Comparison between core temperature during 24 hours of hypothermia and 6 hours of rewarming for mattress temperature of $42.0^{\circ}C$ for room temperature of $25.0^{\circ}C$ and $20.0^{\circ}C$.

423 The above figure shows a decrease of $5^{\circ}C$ in the room temperature reduces
 424 the minimum value of the core temperature to $33^{\circ}C$ after a 24 hour treatment.
 425 The rewarming rate for subcase B is $0.42^{\circ}C/hour$, 8.5% lower than the original
 426 case for external temperature of $25^{\circ}C$.

427 The fourth case considers the anatomical geometry shown in Figure 1 for
 428 direct blood cooling. The simulation of an invasive procedure using an intravas-
 429 cular catheter uses an insulated mattress during the first hour of simulation
 430 and a room temperature of $25^{\circ}C$. The blood cooling procedure is treated as an
 431 external device with capacity of $100W$ applied during the first hour of simula-
 432 tion. After the first hour, the mattress temperature is set to $33^{\circ}C$ with a heat
 433 transfer coefficient of $10W/m^2.^{\circ}C$ and the intravascular catheter is turned off.
 434 Results of arterial temperature during 24 hours are shown in Fig. 15.

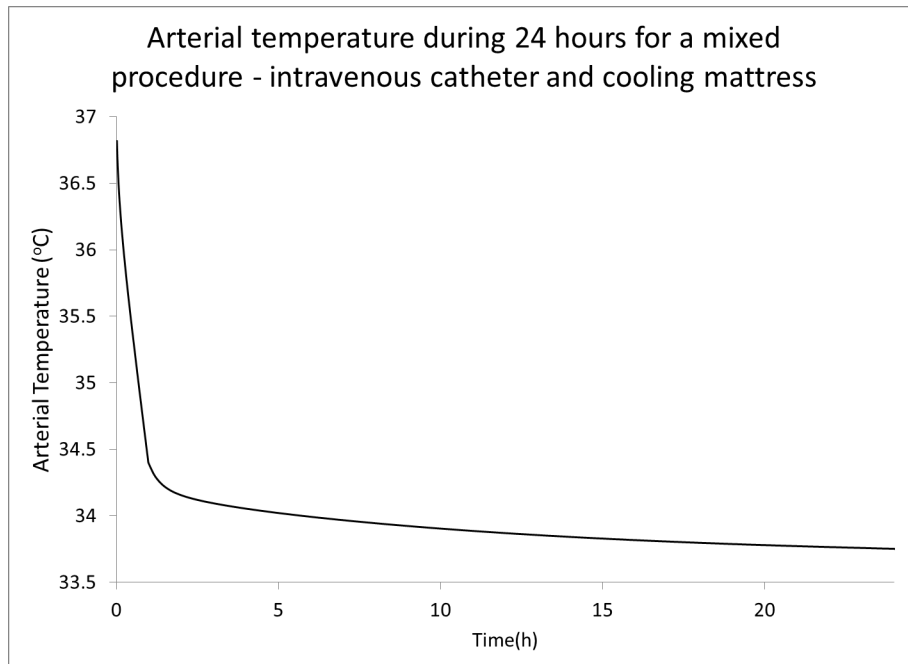


Figure 15: Fourth case: Arterial temperature during 24 hours of a mixed hypothermia procedure - intravenous catheter and cooling mattress.

435 The results show a drop in arterial temperature of $2.6^{\circ}C$ during the first hour
 436 of simulation. After this period, the cooling rate is reduced and the temperature
 437 drops from $34.4^{\circ}C$ to $33.6^{\circ}C$ during the next 23 hours of simulation.

438 5. Conclusion

439 The main goal of the work described in this paper was to develop a finite ele-
 440 ment model able to simulate bioheat transfer processes in adults, and to per-
 441 form whole body cooling procedures as a treatment for brain traumas. The
 442 Pennes bioheat model was chosen to simulate the bioheat transfer processes
 443 in a macroscale and the blood pool approach described in [Fiala, 1998] was
 444 considered to take into account changes in the arterial temperature due to the
 445 circulatory system and heat transfer with the environment. For blood cool-

446 ing using an intravenous catheter, a blood cooling approach described in [Zhu,
447 Schappeler, Cordero-Tumangday, and Rosengart, 2009] was used.

448 The whole body cooling method applied to the adult body produced sat-
449 isfactory results in reducing brain/core temperature to less than $34^{\circ}C$ in two
450 hours. The moderate hypothermia was maintained for 22 hours with a core
451 temperature around $34.0 - 33.8^{\circ}C$. As stated previously, the brain temperature
452 remained $0.2 - 0.3^{\circ}C$ above/below core temperature during the whole analysis.
453 The mattress had to be set to a temperature of $42^{\circ}C$ to allow a smooth increase
454 of core temperature, at a rate around $0.5^{\circ}C/hour$. Although this value is de-
455 fined as the ideal rewarming rate, [Wang, Olivero, Lanzino, Elkins, Rose, and
456 Honings, 2004] reported values of $0.15 - 1.45^{\circ}C/hour$ measured on randomised
457 trials, showing that the rewarming procedures are not always able to maintain
458 cooling rates close to the ideal value.

459 The blood cooling simulation, considering an intravascular catheter, was able
460 to reduce core temperature to less than $34^{\circ}C$ in one hour. After the intravas-
461 cular catheter was removed, the cooling mattress was set to a temperature of
462 $33^{\circ}C$. The mixed method was able to simulate a hypothermia treatment with
463 rapid cooling and maintenance of cooling at moderate hypothermia levels dur-
464 ing 24 hours. Suggestions of a study using mixed methods, considering head
465 cooling methods to maintain cooling after induction of hypothermia with cold
466 intravenous fluids were mentioned in [Harris, Andrews, Murray, Forbes, and
467 Moseley, 2012], but no results were found in clinical trials mixing blood cooling
468 with WBC methods.

469 The results of different cooling methods demonstrate the importance of the
470 developed model for the study of different cooling procedures. The simulations
471 presented in this work reproduce a hypothermic treatment in a realistic adult
472 body with results similar to values reported in the literature [Harris, Andrews,
473 Murray, Forbes, and Moseley, 2012, Hoque, Chakkarapani, Liu, and Thoresen,
474 2010, Unit, 2006]. This opens the way for the optimization of the treatment on
475 a patient-specific basis.

476 The major limitations in the use of this type of model are associated with

477 the correct definition of the geometry and the input parameters, very important
478 to obtain good results. In the cases discussed here, the FEM mesh was gener-
479 ated based on a geometry obtained from CT scans, so the model for the human
480 body is based on a real geometry. One of the greatest difficulties of the numer-
481 ical model is the determination of the correct parameters to guarantee that the
482 analysis corresponds to the real case, as small differences in some of the param-
483 eters can result in substantial differences in temperature, as demonstrated by
484 the sensitivity analysis in [Silva, Laszczyk, Wrobel, Ribeiro, and Nowak, 2016].
485 A sensitivity analysis performed for a neonate model [Silva, Laszczyk, Wrobel,
486 Ribeiro, and Nowak, 2016] shows the importance of correctly determining input
487 parameters as external temperature and heat transfer coefficient. For the correct
488 determination of parameters, at this stage of the research literature values were
489 used, adapted from other numerical simulations [Vallez, Plourde, and Abraham,
490 2016, Fiala, 1998] and from an experimental database source [Hasgall, Gennaro,
491 Baumgartner, Neufeld, Gosselin, Payne, Klingenbock, and Kuster, 2015].

492 Calibration of the model using real hypothermia cases could be used as a
493 starting point to test cost-effective methods for brain/body cooling. Experi-
494 ments for determination of the convective heat transfer coefficient should be
495 conducted to establish a standard database for bioheat transfer in the human
496 body. After validation, tests of cost-effective methods could be used as a stan-
497 dard protocol in clinics and hospitals for public health care, reducing neurolog-
498 ical damages after cerebral traumas.

499 Although the benefits of hypothermia for post-traumatic brain injuries in
500 adults is widely known, the uncertainties about effectiveness and robust evi-
501 dence of reducing brain temperature during clinical trials makes it difficult to
502 define a cooling method to be used for each case of trauma. Whole body cooling
503 is a promising method that still needs further research and more robust evidence
504 of temperature reduction. Studies should describe clear baseline temperatures,
505 duration of cooling, temperatures achieved and temperature changes with cool-
506 ing, along with side effects of each method. In this way, joint research between
507 engineers and clinicians could fill some empty spaces and collaborate to reduce

508 post-traumatic neurological damage in patients suffering brain traumas.

509 Although the development of this three-dimensional finite element model
510 was conducted with the objective of investigating hypothermia treatments, it
511 can also be adapted to predict body temperature changes during exercises and
512 different heat exposures. The numerical tool presented here can be improved
513 and many additional time or temperature-dependent parameters can be added
514 to simulate transient body temperature on different applications.

515

516 Acknowledgements: We thank the Carlos Chagas Filho Research Foundation of the
517 State of Rio de Janeiro (FAPERJ) and the Coordination for the Improvement of Higher
518 Education Personnel (CAPES), both in Brazil, for the financial support.

519

520 Conflicts of Interest: None

521 Funding: Carlos Chagas Filho Research Foundation of the State of Rio de
522 Janeiro (FAPERJ) and the Coordination for the Improvement of Higher Ed-
523 ucation Personnel (CAPES)

524 Ethical Approval: Not required

525 References

526 M. Al-Othmani, N. Ghaddar, and K. Ghali. A multi-segmented human bioheat
527 model for transient and asymmetric radiative environments. *International*
528 *Journal of Heat and Mass Transfer*, 51:5522–5533, 2008.

529 A. Bhowmik, R. Singh, R. Repaka, and S.C. Mishra. Conventional and newly
530 developed bioheat transport models in vascularized tissues: A review. *Journal*
531 *of Thermal Biology*, 38(3):107–125, 2013.

532 C.W. Callaway, S.C. Tadler, L.M. Katz, C.L. Lipinski, and E. Brader. Feasi-
533 bility of external cranial cooling during out-of-hospital cardiac arrest. *Resus-*
534 *citation*, 52:159–165, 2002.

- 535 M. Christiansen, N. Rakhilin, A. Tarakanova, and K. Wong. Modeling brain
536 cooling treatment approved for hypoxic-ischemic encephalopathy in infants to
537 treat stroke and cardiac arrest in adult patients. Cornell University, 2010.
- 538 M. W. Dae, D. W. Gao, P. C. Ursell, C. A. Stillson, and D. I. Sessler. Safety and
539 efficacy of endovascular cooling and rewarming for induction and reversal of
540 hypothermia in human-sized pigs. *Stroke*, 34:734–738, 2003.
- 541 B. H. Dennis, R. C. Eberhart, G. S. Dulikravich, and S. W. Radons. Finite-
542 element simulation of cooling of realistic 3-d human head and neck. *Journal*
543 *of Biomechanical Engineering*, 125(6):832–840, 2003.
- 544 C. Diao, L. Zhu, and H. Wang. Cooling and rewarming for brain ischemia or
545 injury: Theoretical analysis. *Annals of Biomedical Engineering*, 31(3):346–
546 353, 2003.
- 547 D. J. Eicher, C. L. Wagner, L. P. Katikaneni, T. C. Hulsey, W. T. Bass,
548 D. A. Kaufman, M. J. Horgan, S. Languani, J. J. Bhatia, L. M. Givelichian,
549 K. Sankaran, and J. Y. Yager. Moderate hypothermia in neonatal en-
550 cephalopathy: efficacy outcomes. *Pediatric Neurology*, 32:11–17, 2005.
- 551 D. Fiala. *Dynamic simulation of human heat transfer and thermal comfort*. PhD
552 thesis, De Montfort University, Leicester, UK, 1998.
- 553 D. Fiala, K. J. Lomas, and M. Stohrer. A computer model of human thermoreg-
554 ulation for a wide range of environmental conditions: the passive system.
555 *Journal of Applied Physiology*, 87(5):1957–1972, 1999.
- 556 D. Fiala, G. Havenith, P. Bröde, and G. Jendritzky B. Kampmann. UTCI-
557 fiala multi-node model of human heat transfer and temperature regulation.
558 *International Journal of Biometeorology*, 56(3):429–441, 2012.
- 559 C. J. Gordon. The therapeutic potential of regulated hypothermia. *Emergency*
560 *Medicine Journal*, 18(2):81–89, 2001.

- 561 B. Harris, P.J.D. Andrews, G.D. Murray, J. Forbes, and O. Moseley. Systematic
562 review of head cooling in adults after traumatic brain injury and stroke. *Health*
563 *Technology Assessment*, 16(45):1–175, 2012.
- 564 O.A. Harris, C.R. Muh, M.C. Surles, Y. Pan, G. Rozycki, and J. Macleod.
565 Discrete cerebral hypothermia in the management of traumatic brain injury:
566 a randomized controlled trial. *Journal of Neurosurgery*, 110(6):1256–1264,
567 2009.
- 568 P. A. Hasgall, F. Di Gennaro, C. Baumgartner, E. Neufeld, M. C. Gosselin,
569 D. Payne, A. Klingenbock, and N. Kuster. IT’IS database for thermal and
570 electromagnetic parameters of biological tissues. Virtual Population Group,
571 2015.
- 572 R. W. Hickey and M. J. Painter. Brain injury from cardiac arrest in children.
573 *Neurologic Clinics*, 24:147–158, 2006.
- 574 N. Hoque, E. Chakkarapani, X. Liu, and M. Thoresen. A comparison of cooling
575 methods used in therapeutic hypothermia for perinatal asphyxia. *Pediatrics*,
576 126:e124–e130, 2010.
- 577 T. J. Hughes. *The Finite Element Method - Linear Static and Dynamic Finites*
578 *Element Analysis*. Prentice-Hall International Editions, New Jersey, 1987.
- 579 B. R. Kingma, M. J. Vosselman, A. J. Frijns, A. A. Van Steenhoven, and W. D.
580 Van Marken Lichtenbelt. Incorporating neurophysiological concepts in math-
581 ematical thermoregulation models. *International Journal of Biometeorology*,
582 58(1):87–99, 2014.
- 583 J. E. Laszczyk and A. J. Nowak. *The analysis of a newborn’s brain cooling pro-*
584 *cess - measurements and CFD modelling*. LAP LAMBERT Academic Pub-
585 lishing, Gliwice, 2015a.
- 586 J. E. Laszczyk and A. J. Nowak. Computational modelling of neonates brain
587 cooling. *International Journal of Numerical Methods for Heat and Fluid Flow*,
588 26(2):571–590, 2015b.

- 589 G. M. J. Van Leeuwen, J. W. Hand, J. J. W. Lagendijk, D. V. Azzopardi, and
590 A. D. Edwards. Numerical modeling of temperature distributions within the
591 neonatal head. *Pediatric Research*, 48(3):351–356, 2000.
- 592 A. Nozari, P. Safar, S. W. Stezoski, X. Wu, S. Kostelnik, A. Radovsky, S. Tisher-
593 man, and P. M. Kochanek. Critical time window for intra-arrest cooling with
594 cold saline flush in a dog model of cardiopulmonary resuscitation. *Journal of*
595 *the American Heart Association*, 113:2690–2696, 2006.
- 596 A. B. C. G. Silva. *Numerical analyses of the temperature distribution in the*
597 *human brain using the finite element method*. MSc dissertation, Federal Uni-
598 versity of Rio de Janeiro, Rio de Janeiro, Brazil, 2012.
- 599 A. B. C. G. Silva. *A finite element thermoregulation model of the human body for*
600 *hypothermia treatment in adults and neonates*. DSc thesis, Federal University
601 of Rio de Janeiro, Rio de Janeiro, Brazil, 2016.
- 602 A. B. C. G. Silva, J. Laszczyk, Luiz C. Wrobel, F. L. B. Ribeiro, and A. J.
603 Nowak. A thermoregulation model for hypothermic treatment of neonates.
604 *Medical Engineering and Physics*, 38:988–998, 2016.
- 605 S. A. Tisherman and F. Sterz. *Therapeutic Hypothermia*. Springer, San Fran-
606 cisco, 2005.
- 607 National Perinatal Epidemiology Unit. TOBY study protocol - whole body hy-
608 pothemia for the treatment of perinatal asphyxial encephalopathy. volume 2.
609 National Perinatal Epidemiology Unit, 2006.
- 610 L. J. Vallez, B. D. Plourde, and J. P. Abraham. A new computational thermal
611 model of the whole human body: Applications to patient warming blankets.
612 *Numerical Heat Transfer - Part A*, 69(3):227–241, 2016.
- 613 H. Wang, W. Olivero, G. Lanzino, W. Elkins, J. Rose, and D. Honings. Rapid
614 and selective cerebral hypothermia achieved using a cooling helmet. *Journal*
615 *of Neurosurgery*, 100:272–277, 2004.

- 616 S. Hai Xiang and J. Liu. Comprehensive evaluation on the heating capacities of
617 four typical whole body hyperthermia strategies via compartmental model.
618 *International Journal of Heat and Mass Transfer*, 51:5486–5496, 2008.
- 619 Y. Yang, X. Ou, and Q. Chen. A study on time of head hypothermy for large
620 acreage cerebral infarction patients with central high fever. *Chinese Nursery*,
621 20:45–46, 2006.
- 622 L. Zhu and C. Diao. Theoretical simulation of temperature distribution in the
623 brain during mild hypothermia treatment for brain injury. *Medical Biological*
624 *Engineering Computing*, 39(6):681–687, 2001.
- 625 L. Zhu, T. Schappeler, C. Cordero-Tumangday, and A. J. Rosengart. Thermal
626 interactions between blood and tissue. *Advances in Numerical Heat Transfer*,
627 3:191–219, 2009.